IEEE Access
Multidisciplinary ⋮ Rapid Review ⋮ Open Access Journal

Received 11 December 2023, accepted 17 January 2024, date of publication 26 January 2024, date of current version 13 February 2024.

Digital Object Identifier 10.1109/ACCESS.2024.3358810

RESEARCH ARTICLE

Design of a Shared-Aperture Dual-Loop Antenna Using a Mutual Complementary Shape to Improve an Electromagnetic Transparent Characteristics Between S/X-Band Elements

DOYOUNG JANG[1], SUNGSIK WANG[2], HYUN KIM[3], AND HOSUNG CHOO[1], (Senior Member, IEEE)

[1]Department of Electronic and Electrical Engineering, Hongik University, Seoul 04066, South Korea
[2]Department of Electrical, Electronic, & Communication Engineering, Hanyang Cyber University, Seoul 04066, South Korea
[3]Radar Research and Development, LIG Nex1 Company, Yongin-si 16911, South Korea

Corresponding author: Hosung Choo (hschoo@hongik.ac.kr)

This work was supported by the Challenging Future Defense Technology Research and Development Program of the Agency for Defense Development in 2019 under Grant 9127786.

ABSTRACT In this paper, we propose an S/X-band shared-aperture array antenna with a mutual complementary design to improve the electromagnetic (EM) transparent characteristics. A unit-cell of the proposed antenna includes one dual-loop element for the S-band and 3 × 3 dual-loop elements for the X-band. To configure the shared-aperture structure in a limited space, the S-band element is stacked on top of the X-band elements. To solve the practical engineering problems of the shared-aperture antennas, novel design techniques such as using a mutual complementary structure, a coupling compensation array, an interface layer, and an antenna modularization are employed. To verify the antenna feasibility, the fabricated unit-cell extends into a 4 × 4 unit-cell array. The fractional bandwidth of the reflection coefficients for the proposed array are 14.7% and 15% in the S- and X-bands, respectively. In the S-band, as the steering direction of the main beam increases from 0° to 45°, the maximum gain decreases from 14.6 dBi to 11.8 dBi. In the X-band under the same conditions, the maximum gain varies from 26.6 dBi to 25.3 dBi.

INDEX TERMS Array antennas, shared aperture antennas, radar, dual loop antennas, mutual complimentary design.

I. INTRODUCTION

In recent years, the demand for a multi-function radar (MFR) system of military ships that includes both the S- and X-bands is gradually increasing [1], [2], [3], [4]. The MFR is useful for detecting and tracking enemies from a long-distance; however, the drawback of such a system is the fact that both antennas are mounted separately, which means that the mounting area is relatively larger than in conventional radar systems. To minimize the mounting area, shared-aperture antennas technologies can be considered an attractive solution for MFR applications. Thus, combinations of various elements for the shared-aperture antennas such as patches, monopoles, loops, and meshed patches [5], [6], [7], [8], [9], [10], [11], have been reported. Since the various elements of the different bands need to be integrated in a limited space, the shared-aperture antennas typically suffer from performance degradation due to the mutual coupling effects caused by adjacent elements. To overcome these mutual coupling effects, various techniques, such as the insertion of

The associate editor coordinating the review of this manuscript and approving it for publication was Tutku Karacolak.

a cavity structure [12], a meta-surface [13], and an electromagnetic band gap structures [14], have been reported. Nevertheless, these technologies have structural difficulties in applying to stacked shared-aperture antennas. In addition, it is important to achieve the electromagnetic (EM) transparent characteristics of the top-placed element with regard to the bottom-placed element. However, the research on the EM transparent characteristics of the shared-aperture radar arrays has not yet been sufficiently conducted.

In this paper, we propose a shared-aperture array antenna with a mutual complementary shape to improve the EM transparent characteristics. A unit-cell of the proposed antenna includes one dual-loop element for the S-band and 3 × 3 dual-loop elements for the X-band. To configure the shared-aperture structure in a limited space, the S-band element is stacked on top of the X-band elements. Then, novel design techniques to solve the practical engineering problems of the shared-aperture antennas are employed in the proposed antenna: the S-band element has a mutual complementary shape, which improves the EM transparent characteristics in the X-band without degradation of the antenna performance. In [15], we reported some preliminary results on the shared-aperture radar arrays using a hashmark-shaped loop, but consideration for the design of the X-band array and the feeding network was not sufficiently described. In addition, the array performance such as an active reflection coefficient (ARC), an array gain, and beam steering has not been explained. In this study, a coupling compensation design is applied to the X-band elements in consideration of the mutual coupling characteristics between the S-band element and each X-band element. This can improve the antenna bandwidth in the multilayered shared-aperture array. Then, an interface layer is applied under the X-band layer to enhance the antenna durability. To improve maintainability, the unit-cell of the proposed antenna is modularized in a symmetrical structure, where the full radar array can be obtained through repeated arrangement of the modules. To verify the antenna feasibility, the reflection coefficients are investigated in the S- and X-bands. Furthermore, the proposed unit-cell expands into a 4 × 4 unit-cell array to examine the array performance such as the ARC, the array gain, and beam steering. The results demonstrate that the proposed shared-aperture antenna is suitable for MFR applications.

II. DESIGN OF THE HASHMARK-SHAPED ANTENNA

Figure 1 illustrates the geometry of the S/X-band multilayered shared-aperture array antenna for the MFR systems. The unit-cell of the proposed antenna consists of one S-band element and 3×3 X-band elements array. A coupled-fed dual-loop structure is employed for the X-band elements (Layer 1 and Layer 2), which can achieve a broadband matching characteristic. To improve the isolation of the X-band elements, via cavity structures are inserted among them. The width, length, and thickness of the X-band elements are w_{xij}, l_{xij}, and t_{xij}, respectively, where i and j indicate the element number and the layer number, respectively. The S-band elements with the coupled-fed structure (Layer 3 and Layer 4) are stacked on top of the X-band elements so that the S- and X-band elements share a limited aperture space. Herein, when placing the S-band elements above the X-band elements, there are several advantages compared to the opposite case. One S-band element has a smaller total radiator area than nine X-band elements in the unit-cell, which means that the S-band element results in a smaller blockage effect. In addition, since the feeding structure of the X-band elements is more complicated than that of the S-band elements, it is preferred that X-band elements are placed at the bottom. Nevertheless, in this stacked configuration, the S-band element still physically blocks the X-band elements, which causes performance degradation in the X-band. To overcome this blockage effect without degrading the antenna bandwidth, the S-band element has a mutual complementary shape for obtaining the EM transparent characteristics in the X-band. The lengths of the conductors extending into the x and y axis from the loop edge are a_{ij} and b_{ij}. The width, length, and thickness of the S-band elements are w_{sij}, l_{sij}, and t_{sij}, respectively. A perforated layer ensuring the presence of an air gap is placed between the S- and X-band layers, which can minimize the manufacturing errors by providing a soldering space of h_{air}. The thicknesses of the antenna layers are h_1, h_2, h_3, and h_4 from the bottom. For the electric beam steering, the proposed shared-aperture antenna should be connected to the transmitting receiver modules (TRMs). Due to the harsh operating environment of a military ship, the connection between the antenna part and the TRMs must be robust with regard to the external shocks. Therefore, an interface layer is employed between the antenna part and the TRMs, which prevents any unwanted movement of the feed-pin due to the external shocks as shown in Figure 1(d) [16], [17]. The geometric parameters are optimized using a genetic algorithm and the FEKO EM simulator [18], [19], and they are listed in Table 1. This optimization requires more than 96 hours with 128 GBytes of memory (AMD Ryzen 7 3700X, 8 core processor). A simple cost function of 1/bandwidth is used for the optimization process.

Figure 2 shows the pattern distortion in the X-band element according to the size of the S-band element. As shown in Figure 2(a), the S-band element is located above the nine X-band elements, which causes the pattern distortion of the X-band elements. The effects of the S-band element on the X-band elements vary according to their relative locations. The pattern distortion of the X-band element is defined by the following equation:

$$PD(\text{dB}) = 10\log_{10}\frac{\int_0^{2\pi}\int_0^{\frac{\pi}{2}} |F_o(\theta,\phi) - F_l(\theta,\phi)|\,\sin\theta d\theta d\phi}{2\pi} \tag{1}$$

where the F_o means the radiation gain pattern of the X-band patch antenna without the S-band element, and F_l is the radiation gain pattern with the S-band element. Therefore, the PD is defined as the difference between the F_o and the F_l,

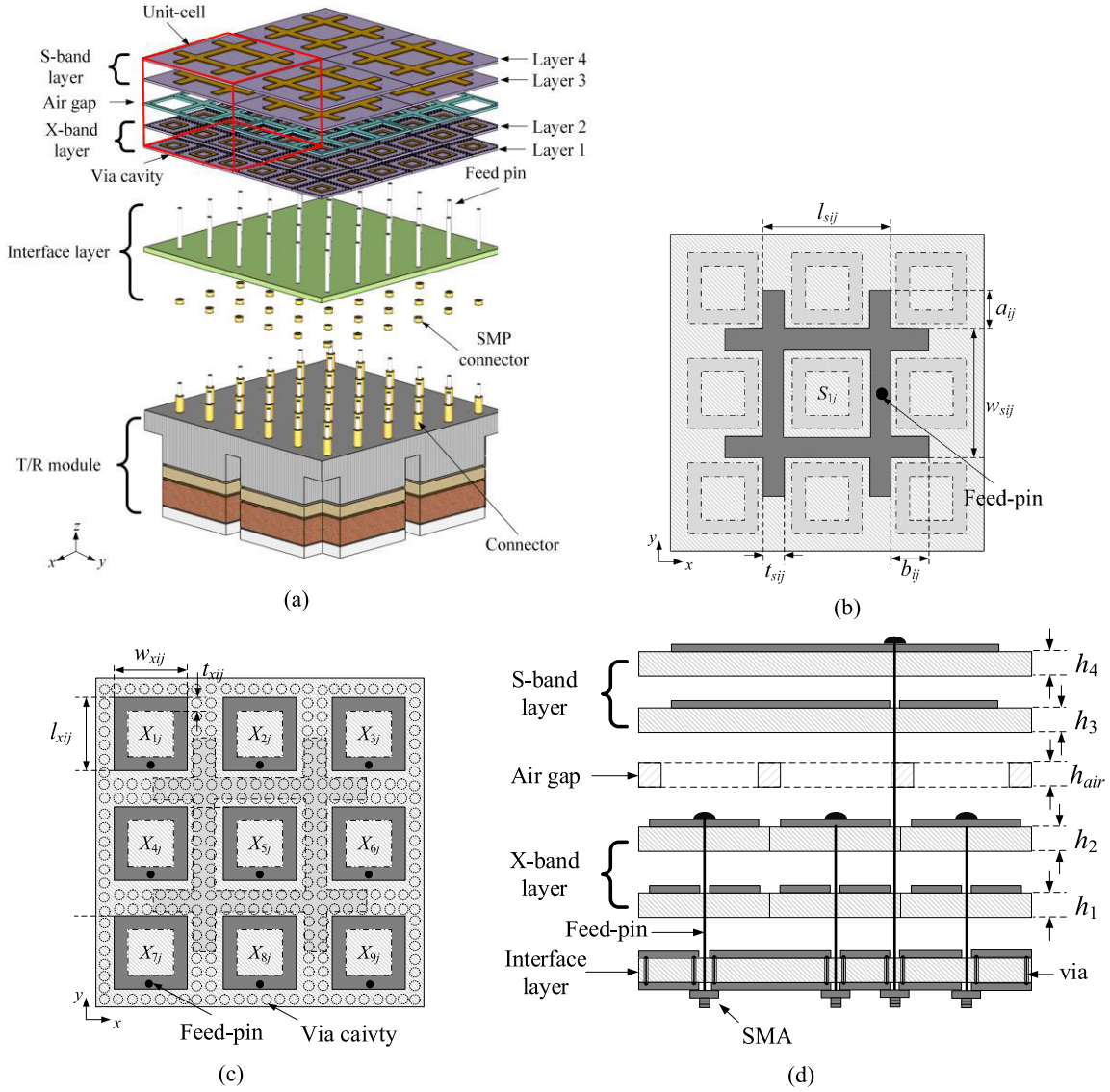

FIGURE 1. Geometry of the proposed antenna. (a) 2 × 2 unit-cell array, (b) S-band layer, (c) X-band layer, and (d) side view of the unit-cell.

where the *PD* is observed in front half space of the antenna. As the variable *s* (S-band element size) increases, the *PD* of the element located on the side (p_8) also increases, as shown in Figure 2(b). On the other hand, as the variable s decreases, the *PD* of the central element (p_5) becomes higher than that of the side elements.

Figure 3 presents the coupling compensated design of the X-band array. The bandwidth characteristics of the X-band elements are degraded due to the mutual coupling with the S-band element. Since the coupling characteristics between the S-band and X-band elements differ depending on their relative distances, the coupling effects should be differently compensated for each X-band element. Therefore, a correction length of l_m is applied to the basic X-band loop for the purpose of the coupling compensation, as shown in Figure 3(a). Thus, the X-band array antennas of the proposed array have non-uniform element sizes, as shown in Figure 3(b). Figure 3(c) shows the fractional bandwidth characteristics with and without the coupling compensation technique. When the coupling compensation is not applied, the bandwidth of each element is not uniform, and the average fractional bandwidth is 12%. On the other hand, when the coupling compensation is applied, the average fractional bandwidth is improved up to 15%.

III. VERIFICATION OF THE PROPOSED ANTENNA

Figure 4. illustrates the fabricated array antenna. To verify the antenna feasibility, the proposed unit-cell is fabricated and extended into a 4 × 4 array configuration. The array spacings in the S- and X-band arrays are 51 mm (0.52λ

TABLE 1. Optimized design parameters.

Parameters	Values (mm)	Parameters	Values (mm)	Parameters	Values (mm)
w_{x11}	6.1	w_{x21}	5.1	w_{x41}	4.6
w_{x51}	5.5	w_{x12}	9.1	w_{x22}	9.1
w_{x42}	7.6	w_{x52}	3.7	l_{x11}	5.6
l_{x21}	6	l_{x41}	5.3	l_{x51}	9.2
l_{x12}	7	l_{x22}	7	l_{x42}	6.7
l_{x52}	9	t_{x11}	1.1	t_{x12}	1.1
w_{s13}	14.9	w_{s14}	14	l_{s13}	24
l_{s14}	26.1	t_{s13}	1.8	t_{s14}	1.8
a_{13}	0.5	a_{14}	0.3	b_{13}	0.1
b_{14}	1.5	h_1	1.6	h_2	2.4
h_{air}	0.2	h_3	2.4	h_4	4

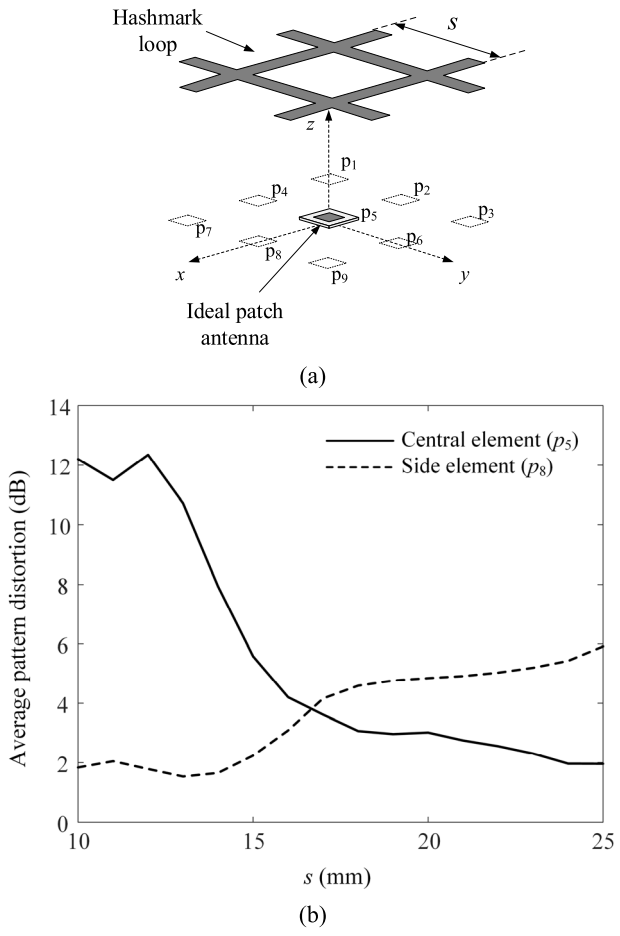

FIGURE 2. Pattern distortion of the X-band element according to the S-band loop size. (a) X-band array and S-band element and (b) average pattern distortion.

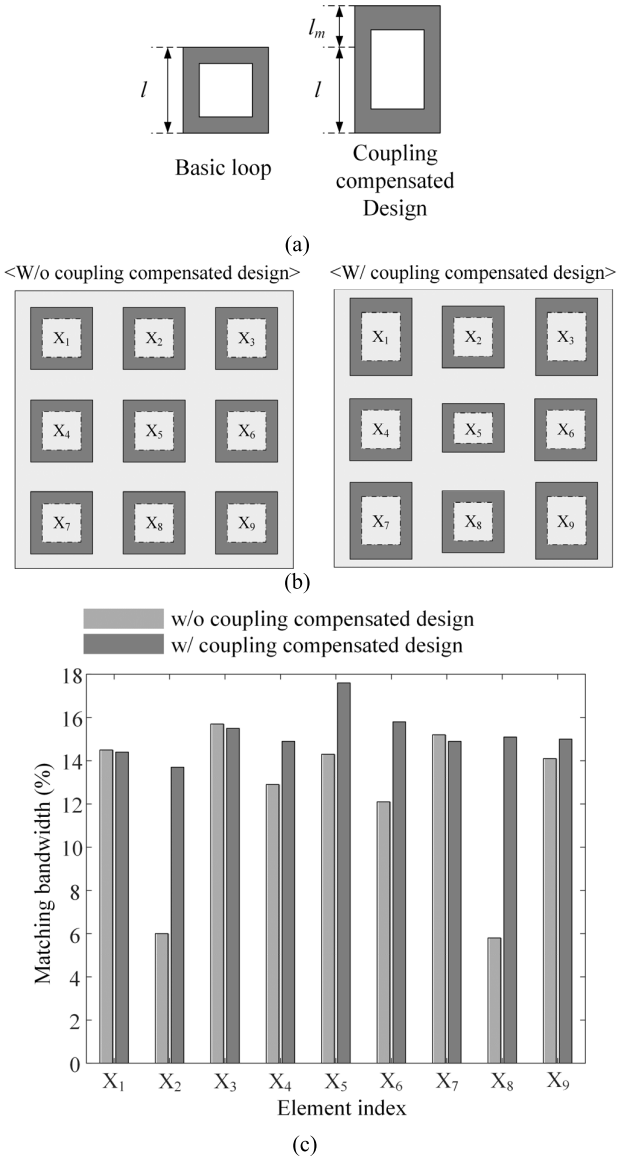

FIGURE 3. Bandwidth with and without the coupling compensated design. (a) basic loop and coupling compensated loop, (b) with and without coupling compensated array configuration, and (c) fractional matching bandwidth of each X-band element.

at 3.05 GHz) and 17 mm (0.54λ at 9.5 GHz), respectively. As can be seen in Figure 4(a), the fully extended array configuration is connected to the TRM part for the purpose of electric beam steering. Figure 4(b) presents the top view of the fabricated S-band layer which contains 4 × 4 S-band array elements. Figure 4(c) illustrates the X-band layer which includes 12 × 12 X-band array elements. The size of each X-band element in the unit-cell is not uniform because the coupling compensation technique is employed as explained in Section II. Plastic screws are used to fix the S- and X-band layers, and TLY-5 substrates ($\varepsilon_r = 2.2$, $\tan\delta = 0.0009$) are used for the antenna substrate layers. The interface layer is inserted between the array antenna and the TRM, and this layer is fabricated using the FR-4 substrate ($\varepsilon_r = 4.6$, $\tan\delta = 0.018$), as shown in Figure 4(d). The durability of the antenna is increased by adopting a metal frame for this layer. The antenna performances such as a reflection coefficient, a gain, and a radiation pattern are measured in a full anechoic chamber.

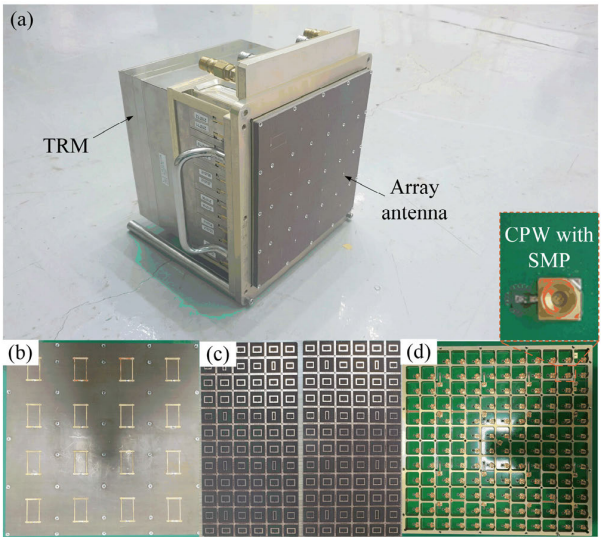

FIGURE 4. Photograph of the fabricated array antenna. (a) isometric view of the assembled radar, (b) top view of the S-band layer, (c) top view of the X-band layer, and (d) bottom view of the antenna part.

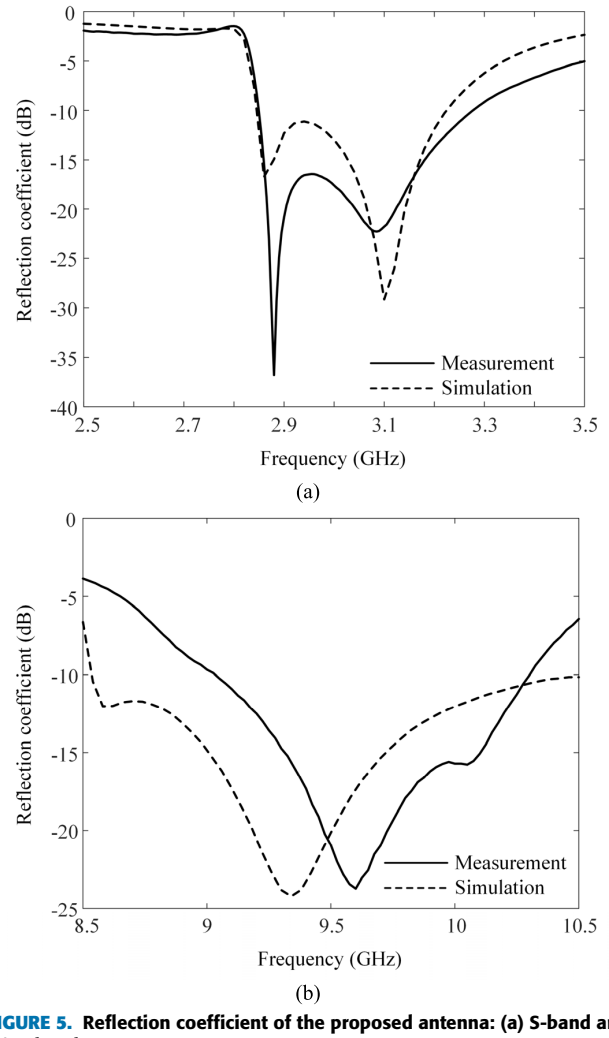

FIGURE 5. Reflection coefficient of the proposed antenna: (a) S-band and (b) X-band.

Figure 5 presents the reflection coefficients for the central element of the S- and X-bands in the array. The reflection

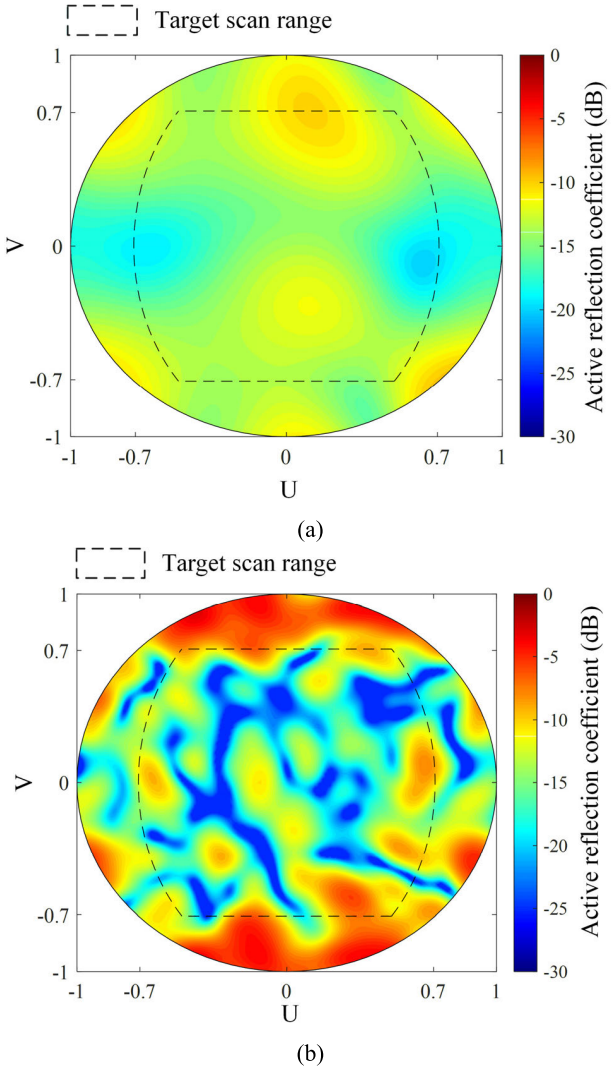

FIGURE 6. Active reflection coefficient of the proposed array: (a) S-band (3.05 GHz) and (b) X-band (9.5 GHz).

coefficients are observed for the central element, and all other elements are terminated with matched loads. The reflection coefficient of the S-band element has a bandwidth of 450 MHz (2.85 GHz to 3.3 GHz, $|\Gamma| < -10$ dB) with a fractional bandwidth of 14.7%, which reveals good agreement with the simulated result of 12.1%, as shown in Figure 5(a). In addition, the fractional bandwidth for the X-band is 15% (8.9 GHz to 10.4 GHz, $|\Gamma| < -10$ dB), which is also in good agreement with the simulated result of 17%, as shown in Figure 5(b).

Figure 6 shows the measured ARC according to the scan angle, where observation frequencies are the S-band at 3.05 GHz and the X-band at 9.5 GHz. The scan range is within $-90°$ to $90°$ in the azimuth angle (AZ) and the elevation angle (EL). The target scan range is determined from $-45°$ to $45°$ in the AZ and EL, which is presented by the dotted line. The target ARC level is determined to be -6 dB for all observation scan range, considering the harsh conditions

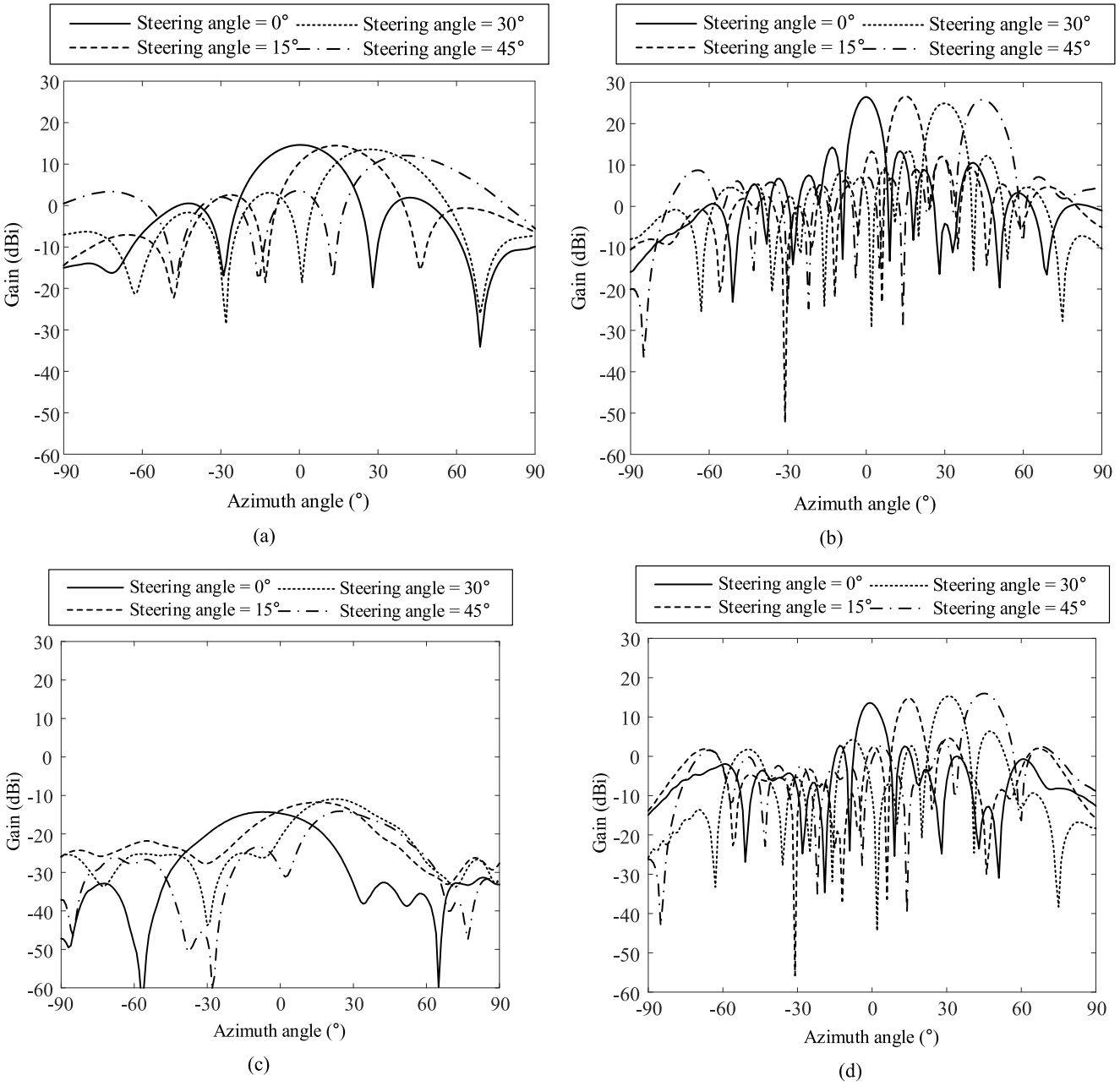

FIGURE 7. Radiation pattern of the proposed array: (a) total gain of the S-band, (b) total gain of the X-band, (c) cross-polarization gain of the S-band, (d) cross-polarization gain of the X-band.

of the multilayered shared-aperture antenna. According to the S-band result, the proposed antenna maintains an ARC of less than −9.8 dB within the target scan area. For the X-band, an ARC of less than −6 dB is observed under the same conditions.

Figure 7 presents the measured array gain when steering the beam at the central frequency of each band. To examine the array gain of the antenna, the active element patterns (AEPs) at all the ports of the proposed array are measured in a full anechoic chamber. The total array gain is then calculated using the AEPs of all the elements based on the following equation [20], [21]:

$$G_{array}(AZ, EL) = \frac{\sum_{i=1}^{I} \bar{w}_i \bar{g}_i (AZ, EL)}{\sqrt{\sum_{i=1}^{I} |w_i|^2}} \tag{2}$$

where g_i is a complex AEP vector of the i_{th} element port, and w_i is a complex weighting vector of the i_{th} element port. Average bore-sight gains of all AEP in the S- and X-bands are 3.7 dBi and 4.8 dBi, respectively. As the main beam

TABLE 2. Comparisons of the proposed antenna.

Research	Bandwidth	Number of Elements	Antenna height	Scan range
[6]	L-band: 8% X-band: 4%	L-band: 12 X-band: 528	30 mm	±15°
[7]	S-band: 11.6% X-band: 18.9%	S-band: 4 X-band: 36	41.7 mm	-
[8]	S-band: 29.6% X-band: 15.5%	S-band: 1 X-band: 9	29 mm	±45°
[9]	S-band: 26.5% X-band: 25.6%	S-band: 1 X-band: 4	11.6 mm	-
[10]	S-band: 25.2% X-band: 19.6%	S-band: 1 X-band: 9	6.1 mm	-
[11]	S-band: 10.8% X-band:14.3%	S-band: 4 X-band: 36	10.7 mm	-
This work	S-band: 14.7% X-band:15%	S-band: 16 X-band: 144	10.6 mm	±45°

steering angle increases from AZ = 0° to 45° in the S-band, the maximum gain decreases from 14.6 dBi to 11.8 dBi. The side lobe level (SLL) also decreases from 12.7 dB to 11.3 dB, as shown in Figure 7(a). In the X-band, the maximum gain varies from 26.6 dBi to 25.3 dBi under the same conditions, and the SLL also decreases from 14.3 dB to 12.7 dB, as shown in Figure 7(b). In addition, the beam steering performances are examined at narrower intervals, confirming that scan blindness does not occur within the target steering range. Figures 7(c) and (d) indicate the cross-polarization gains of the proposed antenna. The maximum cross-polarization levels are −10.92 dBi in the S-band and 16 dBi in the X-band, respectively. The antenna performances are then compared with other studies in Table 2. The proposed array has a low antenna height while having a bandwidth of more than 10% in each band. In addition, the proposed array is designed considering the high durability and easy maintenance compared to other studies. The array gain and ARC are investigated by steering the beam up to ±45° in the azimuth and elevation directions. These results demonstrate that the proposed shared aperture antenna is suitable for MFR applications.

IV. CONCLUSION

We investigated the S/X-band shared-aperture array antenna with the hashmark-shaped element to improve the EM transparent characteristics. To configure the unit-cell of the shared-aperture structure in the limited space, the one S-band element with the hashmark-shaped loop was stacked on top of the 3 × 3 X-band dual-loop array. To verify the antenna feasibility, the proposed unit-cell was fabricated and extended into 4 × 4 unit-cell array configuration. The fractional bandwidth of the reflection coefficients of the S- and X-bands were 14.7% and 15%, respectively. In addition, when the array beam was steered from −45° to 45° in the AZ and EL, the ARCs of the S- and X-bands were observed to be less than −9.8 dB and −6 dB, respectively. When the main beam steering angle was increased from AZ = 0° to 45° in the S-band, the maximum gain decreased from 14.6 dBi to 11.8 dBi. Then, the SLL also decreased from 12.7 dB to 11.3 dB. In the X-band under the same condition, the maximum gain varied from 26.6 dBi to 25.3 dBi, while the SLL decreased from 14.3 dB to 12.7 dB. These results demonstrated that the proposed shared-aperture antenna was suitable for MFR applications. Therefore, the research of this paper will help to solve the practical engineering problems of the MFRs of the shared-aperture configuration.

REFERENCES

[1] S. Gauthier, E. Riseborough, T. J. Nohara, and G. Jones, "Multifunction radar simulator (MFRSIM)," Defence R&D Canada, Ottawa, ONT, Canada, Tech. Rep., TM 2011–207, 1993, pp. 2–10.

[2] Y. Zhou, T. Wang, R. Hu, H. Su, Y. Liu, X. Liu, J. Suo, and H. Snoussi, "Multiple kernelized correlation filters (MKCF) for extended object tracking using X-band marine radar data," *IEEE Trans. Signal Process.*, vol. 67, no. 14, pp. 3676–3688, Jul. 2019.

[3] A. Wang and V. Krishnamurthy, "Signal interpretation of multifunction radars: Modeling and statistical signal processing with stochastic context free grammar," *IEEE Trans. Signal Process.*, vol. 56, no. 3, pp. 1106–1119, Mar. 2008.

[4] W. N. Dawber and N. M. Harwood, "Comparison of Doppler clutter cancellation techniques for naval multi-function radars," in *Proc. RADAR*, Edinburgh, U.K., 2002, pp. 424–428.

[5] P. Mei, S. Zhang, and G. F. Pedersen, "A dual-polarized and high-gain X-/Ka-band shared-aperture antenna with high aperture reuse efficiency," *IEEE Trans. Antennas Propag.*, vol. 69, no. 3, pp. 1334–1344, Mar. 2021.

[6] Y. Chen and R. G. Vaughan, "Dual-polarized L-band and single-polarized X-band shared-aperture SAR array," *IEEE Trans. Antennas Propag.*, vol. 66, no. 7, pp. 3391–3400, Jul. 2018.

[7] K. Li, T. Dong, and Z. Xia, "A broadband shared-aperture L/S/X-band dual-polarized antenna for SAR applications," *IEEE Access*, vol. 7, pp. 51417–51425, 2019.

[8] S. Wang, H. Kim, D. Kim, and H. Choo, "Multi-band array antenna sharing a common aperture with heterogeneous array elements," *Appl. Sci.*, vol. 12, no. 18, p. 9348, Sep. 2022.

[9] S. Wang, D. Jang, Y. Kim, and H. Choo, "Design of S/X-band dual-loop shared-aperture 2×2 array antenna," *J. Electromagn. Eng. Sci.*, vol. 22, no. 3, pp. 319–325, May 2022.

[10] S. Wang, H. Kim, H. Kim, and H. Choo, "Design of a polarization-selective EM transparent mesh-type E-shaped antenna for shared-aperture radar applications," *Appl. Sci.*, vol. 12, no. 4, p. 1862, Feb. 2022.

[11] J. Kim, S. K. Hong, and B. Kim, "A shared-aperture S/X dual broadband microstrip antenna with one perforated patch," *Microw. Opt. Technol. Lett.*, vol. 62, no. 1, pp. 507–513, Jan. 2020.

[12] D.-F. Guan, Z.-P. Qian, Y.-S. Zhang, and Y. Cai, "Novel SIW cavity-backed antenna array without using individual feeding network," *IEEE Antennas Wireless Propag. Lett.*, vol. 13, pp. 423–426, 2014.

[13] J. Guo, F. Liu, L. Zhao, Y. Yin, G.-L. Huang, and Y. Li, "Meta-surface antenna array decoupling designs for two linear polarized antennas coupled in H-plane and E-plane," *IEEE Access*, vol. 7, pp. 100442–100452, 2019.

[14] H. S. Farahani, M. Veysi, M. Kamyab, and A. Tadjalli, "Mutual coupling reduction in patch antenna arrays using a UC-EBG superstrate," *IEEE Antennas Wireless Propag. Lett.*, vol. 9, pp. 57–59, 2010.

[15] D. Jang, S. Wang, S. Kim, D. Kim, and H. Choo, "Design of a shared-aperture antenna with a hashmark-shaped loop to improve electromagnetic transparent characteristics," in *Proc. Int. Symp. Antennas Propag. (ISAP)*, Oct. 2022, pp. 187–188.

[16] J. Cho, D. Jang, C.-H. Lee, and H. Choo, "Design of an interface layer using CPW between an array antenna and TRM in X-band radar systems to minimize leakage fields and improve transmission characteristics," *Appl. Sci.*, vol. 12, no. 17, p. 8514, Aug. 2022.

[17] D. Jang, T. H. Lim, D. Kim, S. Wang, and H. Choo, "Design of a high-durability X-band patch antenna with a CPW feeding network based on a durability evaluation analysis," *Electronics*, vol. 11, no. 4, p. 553, Feb. 2022.

[18] (2022). *FEKO, Altair*. [Online]. Available: www.altair.com

[19] A. Hassanat, K. Almohammadi, E. Alkafaween, E. Abunawas, A. Hammouri, and V. B. S. Prasath, "Choosing mutation and crossover ratios for genetic algorithms—A review with a new dynamic approach," *Information*, vol. 10, no. 12, p. 390, Dec. 2019.

[20] A. K. Bhattacharyya, *Phased Array Antennas*. Hoboken, NJ, USA: Wiley, 2006.
[21] D. F. Kelley and W. L. Stutzman, "Array antenna pattern modeling methods that include mutual coupling effects," *IEEE Trans. Antennas Propag.*, vol. 41, no. 12, pp. 1625–1632, Dec. 1993.

DOYOUNG JANG received the B.S. degree in information and telecommunication engineering from Dongyang Mirae University, Seoul, Republic of Korea, in 2018, and the M.S. and Ph.D. degrees in electronic and electrical engineering from Hongik University, Seoul, in 2020 and 2023, respectively. He was a Research Engineer with MOASOFT, Seoul, from 2015 to 2018. He is currently a Research Professor with the Metamaterial Electronic Component Research Center, Hongik University. His research interests include array antennas, radars, and electromagnetic wave propagation.

SUNGSIK WANG received the B.S. and M.S. degrees in radio science and engineering from Hanyang University, Seoul, South Korea, in 1997 and 1999, respectively, and the Ph.D. degree from the Department of Electronic and Electrical Engineering, Hongik University, in 2021. In September 2021, he joined the Department of Electrical, Electronic, & Communication Engineering, Hanyang Cyber University, Seoul, where he is currently an Assistant Professor. His research interests include beam propagation under abnormal atmospheric phenomenon, broadband antenna design, the use of the optimization algorithm in developing antennas, and antenna array beamforming.

HYUN KIM received the B.S., M.S., and Ph.D. degrees in electrical and electronics engineering from Yonsei University, Seoul, South Korea, in 2002, 2005, and 2011, respectively. He is currently a Research Engineer with LIG Nex1 Company, South Korea. His main research interests include the area of numerical analysis, phased array antenna, and radar systems.

HOSUNG CHOO (Senior Member, IEEE) received the B.S. degree in radio science and engineering from Hanyang University, Seoul, in 1998, and the M.S. and Ph.D. degrees in electrical and computer engineering from The University of Texas at Austin, in 2000 and 2003, respectively. In September 2003, he joined the Department of Electronic and Electrical Engineering, Hongik University, Seoul, South Korea, where he is currently a Professor. His principal area of research interests include electrically small antennas for wireless communications, reader, and tag antennas for RFID, on-glass and conformal antennas for vehicles and aircraft, and array antennas for GPS applications.